Distance Dependence of the Reaction Rate for the Reduction of Metal Cations by Solvated Electrons: A Picosecond Pulse Radiolysis Study

ARTICLE *in* THE JOURNAL OF PHYSICAL CHEMISTRY A · OCTOBER 2010

Impact Factor: 2.69 · DOI: 10.1021/jp107278w · Source: PubMed

Distance Dependence of the Reaction Rate for the Reduction of Metal Cations by Solvated Electrons: A Picosecond Pulse Radiolysis Study

Uli Schmidhammer,[†] Pascal Pernot,[†] Vincent De Waele,[†] Pierre Jeunesse,[†] Alexandre Demarque,[†] Shigeo Murata,[‡] and Mehran Mostafavi*[,†]

Laboratoire de Chimie Physique-ELYSE, UMR8000 CNRS, Université Paris Sud, 91405 Orsay, France and National Institute of Advanced Industrial Science and Technology, AIST Tsukuba Central 5, 1-1-1 Higashi, Tsukuba 305-8565, Japan

Received: August 3, 2010; Revised Manuscript Received: September 30, 2010

The decay of the solvated electron generated by picosecond electron pulse radiolysis is studied by broadband transient absorption measurements in ethylene glycol solutions containing decimolar concentrations of Cu^{2+}, Ni^{2+}, and Pb^{2+} metal cations. Analysis of the nonexponential kinetics of the decays reveals molecular parameters of the electron transfer reaction. It is found that the reaction occurs at long distance for Cu^{2+} solutions and is only limited to contact distance in the case of Ni^{2+} solutions. The distribution of reaction distance strongly depends on the free enthalpy change of the reactions.

I. Introduction

The direct spectroscopic observations in 1962 by E. J. Hart and J. W. Boag of transient solvated electrons produced by pulse radiolysis of aqueous solutions[1] opened the way to an extensive investigation on the properties and theoretical models of the solvated electron (e_s^-). Since then, the rates and mechanisms of the solvated electron reactions with a wide variety of solutes and in many solvents have been studied using time-resolved absorption techniques.[2−7] Actually, this so simple but nevertheless peculiar species is still motivating physical chemists to challenging theoretical and experimental studies.[8,9] Indeed, as a transient species in most solvents at ambient conditions, research on the solvated electron has not only benefited from the technical development on time resolution but also motivated it to a certain extent because it is a very important reducing agent: its reduction potential is very negative. The value of $E°(H_2O/e_s^-)$ for the solvated electron in water is equal to −2.87 V with respect to the standard hydrogen electrode.

With its intense optical absorption in the visible and near-infrared spectral regions, the solvated electron is most conveniently and reliably observed directly by transient absorption spectroscopy where the ionization is made by a short pulse of accelerated electrons (pulse radiolysis) or by an intense short laser pulse (photolysis). Thus, the majority of rate constants of reactions between the solvated electron and solutes, also named electron scavengers, have been determined from the measurement of the solvated electron decay and analysis of the concentration dependence of its kinetics. Many reactions of the solvated electron with various solutes, such as metal cations and their complex, aliphatic, aromatic, or heterocyclic compounds, and also anions and cations have been studied.[10]

As for classic bimolecular reactions, the overall reaction of the solvated electron consists of two steps: (i) the diffusive approach of reactants and (ii) the electron transfer reaction. Thus, the rate of encounter with another species and the (first order) electron reaction rate constant determine the lifetime of the solvated electron, which depends strongly on the experimental conditions. When that reaction rate constant is high compared to the diffusion rate constant, the overall reaction is called diffusion controlled. In this case, the temporal evolution of the reaction does not reveal much information about the electron transfer process. When the reaction rate constant is significantly lower than the diffusion rate constant, the reaction kinetics is determined by the thermal activation and information on the thermodynamic reaction parameters can be obtained. In both cases the kinetics of the decays are monoexponential due to the underlying stationary distributions. However, under particular conditions the overall reaction can be even faster than diffusion-controlled reactions. This is observed when the reaction occurs at distances longer than the contact distance of the reactants. In this case, the decay curve of reacting species deviates from an exponential function at short times; this phenomenon is named the transient effect. For the transient effect to be observed, the concentration of one of the reactants must be high enough and the diffusion rate low enough. From the analysis of the nonexponential part of the decay curve, important reaction parameters can be retrieved and lead to a microscopic picture of bimolecular electron transfer reactions. The transient effect observed in the decay is a kinetic manifestation of the distance dependence of the reaction rate. Indeed, as the reaction rate is higher at short distances, the concentration of reactant pairs is depleted first with preference to those with short distances if the diffusion of the reactants is sufficiently slow. This implies a nonstationary distribution of the distance between the reactants leading to a nonexponential reaction kinetics until a level of spatial depletion is reached where long-range electron transfer and diffusion have similar rates.

During the last 20 years, several groups have studied the transient effect on electron transfer reactions via fluorescence quenching in solution with time-resolved techniques.[11−23] Indirect access can be obtained by steady-state measurement of the fluorescence intensity for different quencher concentrations,[24] a technique that was often used in addition to the time-resolved measurements. Generally, the experimentally observed transient effect was analyzed to study the mechanism of the underlying electron transfer for several donor−acceptor pairs

* To whom correspondence should be addressed. E-mail: mehran.mostafavi@u-psud.fr.
[†] Université Paris Sud.
[‡] National Institute of Advanced Industrial Science and Technology.

10.1021/jp107278w
Published on Web 10/22/2010

in polar and nonpolar, liquid and solid solutions. Hereby, the dependence of the rate constant on the donor−acceptor separation was taken into account on the basis of the Marcus equation[25,26] or some phenomenological rate constant.[15,16,27,28] The time-dependent diffusion equation with a distance-dependent sink term was solved numerically, and the solution was used to calculate the electron-donor decay curve. It was fitted to the observed decay curve to determine electron transfer rate constant parameters.

The reactions of the solvated electron are usually considered to be diffusion controlled. In solution, there is no report on the first-order rate constant of the solvated electron at a room temperature independent of the diffusion. In this work, we pay close attention to the reactivity of the solvated electron, the so peculiar "chemical species" and most fundamental electron donor, by studying its ultrafast reaction with highly concentrated metal cations in ethylene glycol, a viscous solvent that makes the diffusion coefficient of the reactants low. Thanks to our electron pulse−probe setup giving a high signal-to-noise ratio and increased spectral flexibility, the transient effect on the decay of the solvated electron could be resolved in the picosecond range. To the best of our knowledge, this is the first study on the transient effect of a ground-state reaction on this time scale as well as the first for the solvated electron at room temperature. The transient effect in the reaction of the solvated electron with homogeneously dispersed metal cations Cu^{2+}, Pb^{2+}, and Ni^{2+} at high concentrations was studied by pulse radiolysis with picosecond time resolution by probing the visible electronic absorption of the solvated electron. The electron transfer reaction rates are extracted from the fit of the transient absorption measurements of the decays with a time-dependent diffusion coefficient equation including a distance-dependent reaction rate. From these measurements and data analysis, we address two important questions: Is any long distance reaction for the solvated electron possible or do the reactions occur only at the contact distance? Do the reaction rates of the solvated electron depend on the free enthalpy change of the reduction reaction?

II. Experimental Section

The ultrafast pulse radiolysis experiments were performed with a broadband pulse−probe setup that was installed on the experimental area EA-1 of the picosecond electron pulse facility ELYSE. The electron accelerator based on the radiofrequency photogun technology is described in detail elsewhere.[29,30] For the present experiments ELYSE was tuned to deliver electron pulses with an energy of 7.5 MeV and a charge of around 4 nC. Recently, single shot electro-optic sampling[31] of the electric field copropagating with the relativistic electron bunch confirmed that ELYSE provides in this configuration electron bunches with a typical pulse duration around 10 ps and a rms shot-to-shot jitter < 1 ps.[32] The measurements were performed at a repetition rate of the accelerator set to 5 or 10 Hz.

The transient absorption pulse−probe setup is based on the laser-electron intrinsic synchronization resulting from the laser-triggered photocathode[33] as detailed elsewhere.[34,35] In the present work, about 1 μJ of the Ti:Sapphire laser was focused into a 3 mm thick sapphire disk to generate a supercontinuum that was used as the optical probe. The intense region around the fundamental laser wavelength was blocked by a dielectric filter (Calflex X, LINOS AG). After passing the optical delay line, a reference signal is split off from the broadband probe. The remaining probe beam was slightly focused into the sample with a lens of focal length = 300 mm. Probe and reference beams were each coupled into an optical fiber, transmitted to a spectrometer (Shamrock SR-303i with grating blazed at 500 nm and 150 L/mm), and dispersed onto a CCD (Newton DU920N-BU, Andor Technologies). Compared to the previous transient absorption configuration,[35] replacement of the photodiodes by a multichannel CCD camera allows a recording of transient spectra independent of the shot-to-shot electron pulse fluctuations. The probe and reference spectra were recorded with and without electron excitation in order to calculate the electron-triggered change of optical density (ΔOD) cleaned from shot-to-shot fluctuations of the probe intensity. Averaging over 10 of such single measurements for a delay step yielded a shot noise limited sensitivity of better than 10^{-3} ΔOD.

All measurements were made in a flowing cell with a 5 mm optical path collinear to the electron pulse propagation. The cell was placed 30 mm away from the output window of the ELYSE vacuum tube, behind a 200 μm thin aluminum mirror. The diameter of the electron bunch at the position of the cell was in the range of 3−4 mm. In the described configuration, it is mainly the electron pulse duration and velocity mismatch between the electron pulse and the slower visible probe pulse during their propagation inside the cell that determines the time resolution. The rise of the absorption signal from 10% to 90% of the maximum value was found to be below 20 ps. The dispersion over the spectral detection range of interest between 460 and 760 nm was 4 ps. The temporal evolution of the transient spectra of each solution was recorded with low single point averaging of 10−20 for each delay step but on the order of 10 times. By this approach potential drifts of the electron source on the time scale of some minutes can be oppressed. The measurements on the solvation dynamics of the excess electron were done with a step width of 2.5 ps. To acquire the transient effect precisely, delay scans on the subnanosecond scale were performed with a step width on the order of 10 ps whereas measurements up to 4 ns with typically 25 ps.

The details of the nanosecond pulse radiolysis setup were reported earlier.[36] Electron pulses of 3 ns duration were delivered by a Febetron 706 accelerator (600 keV electron energy) to samples contained in a quartz suprasil cell through a thin entrance window, 0.2 mm in thickness. The optical path length perpendicular to the electron beam was 1 cm. The dose per pulse was determined from the electronic density of the alcohol and from the initial absorbance of the solvated electron. The concentration of e_s^- at the end of the pulse was around $1-3 \times 10^{-5}$ mol dm^{-3}. The solution was saturated with pure N_2 and changed after every pulse. The absorbance of the transient species was analyzed by means of a classic setup consisting of a xenon lamp, a monochromator, and a photomultiplier connected with a transient digitizer. Four to five measurements of transient absorbance were performed in order to correct the pulse to pulse dose variation and reduce the noise by averaging. Under the experimental conditions, the picosecond pulse radiolysis delivered a dose rate of around 4×10^5 Gy s^{-1} compared to around 7×10^3 Gy s^{-1} of the nanosecond pulse radiolysis.

The perchlorate metal salts (Aldrich) were dissolved in spectrophotometric-grade ethylene glycol (EG, Sigma Aldrich). The dynamic viscosity values of the highly concentrated salt solutions were determined as a product of the density and kinetic viscosity. The kinetic viscosity was measured with an Ubbelohde-type viscometer. These measurements were done at 22.5 °C, the room temperature during picosecond radiolysis experiments.

III. Methods of Calculation and Data Analysis

III.1. Calculation of the Distance-Dependent Electron Transfer Reaction. The method of data analysis employed in this paper is similar to that already described for analysis of

the transient effect observed in fluorescence quenching by electron transfer in polar and nonpolar solvents.[25] It is described here briefly. Suppose the solvated electron e_s^- and scavenger ion are in solution and the decay of e_s^- absorption occurs by reaction with the scavenger as well as by geminate recombination. Then the decay function $P(t)$ of the e_s^- absorption is given by eq 1[25,37]

$$P(t) = S(t)\exp(-4\pi c_0 \int_d^\infty [1 - U(r,t)]r^2\,\mathrm{d}r) \qquad (1)$$

Here, $S(t)$ is the decay function due to geminate recombination. $S(t)$ can be obtained from experiment, and it is given in section IV.1.

The exponential term in eq 1 represents the decay due to the scavenging reaction. c_0 is the scavenger concentration, and d is the distance of the closest approach of e_s^- and the scavenger ion. $U(r,t)$ stands for the survival probability of a e_s^-−scavenger pair at time t that was initially separated by distance r.

It is necessary to know $U(r,t)$ to calculate $P(t)$. In liquid solution, e_s^- and the scavenger ions diffuse and in that case it has been shown that $U(r,t)$ satisfies the following partial differential equation:[38]

$$\frac{\partial U(r,t)}{\partial t} = D\left[\frac{\partial^2}{\partial r^2} + \left(\frac{2}{r} - \frac{Ze^2}{k_B T\varepsilon r^2}\right)\frac{\partial}{\partial r}\right]U(r,t) - k(r)U(r,t) \qquad (2)$$

D is the sum of the diffusion coefficients of e_s^- and the scavenger ion in solution, Ze the charge of the scavenger ion, k_B the Boltzmann constant, T the temperature, ε the solvent dielectric constant, and $k(r)$ the first-order rate constant of the scavenging reaction. The term $Ze^2/k_BT\varepsilon r^2$ is necessary to take into account the electrostatic interaction between e_s^- and the scavenger ion. Due to a possible complexation by the counteranion, the effective charge Z can vary between 1 and 2. The functional form of $k(r)$ is not known, but it may be approximated by an exponential function.

$$k(r) = A\,\exp[-b(r - d)] \qquad (3)$$

A and b are the parameters characterizing the rate constant. $A = k(d)$ and $d = 4$ Å in this paper.

Equation 2 coupled with eq 3 must be solved under appropriate initial and boundary conditions.[25,27] It was solved numerically by the Crank−Nicholson method. In the calculation, both the temporal and spatial regions were divided into 1000 steps. Since $U(r,t)$ changes faster at shorter times, smaller step sizes were employed at shorter times. $U(r,t)$ thus obtained was substituted in eq 1 to calculate $P(t)$. The integral in eq 1 was calculated by the trapezoidal rule.

From eqs 1, 2, and 3 we see that the shape of the decay curve of e_s^- absorption is determined by the four adjustable parameters D, Z, A, and b. The theoretical decay curve eq 1 was fitted to the experimental decay curves by Baysian data analysis (see section III.2).

The distributions $Y(r)$ and $Y(r,t)$ of the reaction distance of e_s^- and the scavenger ions were calculated by eqs 4 and 5[26,27]

$$Y(r) = 4\pi r^2 c_0 k(r) \int_0^\infty q(r,t)P(t)\,\mathrm{d}t \qquad (4)$$

$$Y(r,t) = 4\pi r^2 c_0 k(r) \int_0^t q(r,t)P(t)\,\mathrm{d}t \qquad (5)$$

where $q(r,t) = c(r,t)/c_0$, $c(r,t)$ is the concentration of the scavenger ion at distance r from e_s^- at time t, and c_0 is its bulk concentration. It has been shown that $q(r,t)$ satisfies a partial differential equation similar to eq 2

$$\frac{\partial q(r,t)}{\partial t} = D\left[\frac{\partial^2}{\partial r^2} + \left(\frac{2}{r} + \frac{Ze^2}{k_B T\varepsilon r^2}\right)\frac{\partial}{\partial r}\right]q(r,t) - k(r)q(r,t) \qquad (6)$$

$Y(r)$ is the distribution of reaction distance. $Y(r)\,\mathrm{d}r$ gives the probability of reaction between e_s^- at the center and the scavenger in a shell with radius r from the center and thickness $\mathrm{d}r$, and $Y(r,t)\,\mathrm{d}r$ that up to time t.

$Y(r)$ and $Y(r,t)$ are calculated numerically using eqs 3−5, with the values of the parameters D, Z, A, and b obtained from the fitting scheme described above.

III.2. Method of Bayesian Data Analysis. The sets of model parameters compatible with the experimental data were obtained by Bayesian inference.[39,40] For each ion, a global analysis of the absorption decays for two concentrations was performed, corresponding to a set of 6 parameters: A, b, D, Z, S_1, and S_2. The last two parameters are amplitudes rescaling the model results to the observations. We note that A, b, and to some extent D and Z are independent of the concentration of the electron acceptor.

According to Bayes's theorem, the posterior probability density function (pdf) of the parameters is

$$p(A,b,D,Z,S_1,S_2|Y_1,Y_2) \propto \mathrm{p}(Y_1,Y_2|A,b,D,Z,S_1,S_2)p(A,b,D,Z,S_1,S_2) \qquad (7)$$

where $p(Y_1,Y_2\,|A,b,D,Z,S_1,S_2)$ is the *likelihood* function describing the measurement noise statistics, i.e., the difference between model and observations, and $p(A,b,D,Z,S_1,S_2)$ is the *prior* pdf, defining our state of knowledge about the parameters beforehand.

For transient absorption, we assume that the measurement noise is uniform, Gaussian, and additive

$$Y_i(t_j) = P_i(t_j) + \varepsilon_i;\ i = 1, 2;\ j = 1, N_i \qquad (8)$$

where $P_i(t_j)$ is the model decay for experiment i and $\varepsilon_i \sim N(0,\sigma_i^2)$ is a normal random variable with average 0 and variance σ_i^2.

The Gaussian/normal distribution of measurement noise is used to model the likelihood function. In the present case, we have enough data points to use a version of the Gaussian pdf marginalized over the noise variance of each experiment with prior $p(\sigma_i) \propto 1/\sigma_i$[41]

$$p(Y_1,Y_2|A,b,D,Z,S_1,S_2) = \prod_{t=1,2} p(Y_i|A,b,D,Z,\mathrm{S}_i) = \prod_{t=1,2}\Big(\sum_{j\,=\,1,N_i}(Y_i(t_j)-P_i(t_j))^2\Big)^{-N_i/2} \qquad (9)$$

The prior pdfs are defined from available information. There is no a priori correlation between the values of the parameters; the joint prior pdf can therefore be factorized as a product of single-parameter pdfs

$$p(A,b,D,Z,S_1,S_2) = p(A)p(b)p(D)p(Z)p(S_1)p(S_2) \quad (10)$$

The amplitude of A being unknown, we use for it a loguniform distribution $A \sim \text{Logunif}(10^8,10^{13})$. A similar distribution is used for $S_1 \sim \text{Logunif}(10^1,10^6)$ and $S_2 \sim \text{Logunif}(10^1,10^6)$. We use experimental evidence to constrain D around 0.1, within a factor 1.5 through a log-normal distribution $D \sim \text{LogN}(0.1,1.5)$. Finally, b and Z have been attributed uniform distributions $b \sim \text{Unif}(0,3)$ and $Z \sim \text{Unif}(0,2)$ (Table 1).

A representative sample of the posterior pdf is generated by a Markov Chain Monte Carlo method using a Metropolis−Hastings algorithm.[42] Estimates of the parameters and their correlation matrix are obtained from this sample. As we are not interested in the scale factors S_1 and S_2, inference on the other parameters is obtained with the marginal posterior pdf

$$p(A,b,D,Z|Y_1,Y_2) = \int \mathrm{d}S_1\mathrm{d}S_2 p(A,b,D,Z,S_1,S_2|Y_1,Y_2) \quad (11)$$

IV. Results

IV.1. Picosecond to Nanosecond Evolution of the Solvated Electron in Ethylene Glycol. In order to determine the decay function $S(t)$ of the population of the solvated electron in pure ethylene glycol, we investigated the temporal and spectral evolution of its electronic absorption in the visible from the pico- to nanosecond regime, i.e., the time window of interest for the transient effect. Figure 1a and 1b show transient spectra for delay times designating the two main ultrafast processes after electron excitation, the solvation and the geminate recombination. Below 100 ps, the spectral evolution reveals a shift of a broad absorption band to shorter wavelengths that is typical for solvation processes observed via transient absorption measurements.[43,44] Here, for EG, this blue shift manifests itself by a strong, lasting absorption decay in the red wing and a short, less pronounced absorption increase in the blue wing and around the future maximum (see also Figure 2). The whole process is accompanied by a general narrowing of the band. The corresponding dynamics on a time scale of several tens of picoseconds reflects the diffusive contribution of solvation including long-range reorganization in the viscous, protic medium.[45] Here, the solvation dynamics ends about 50 ps after excitation. The absorption shape and maximum around 575 nm after solvation correspond to the known spectral signature of the solvated electron generated by nanosecond electron radiolysis as well as femtosecond photolysis in ethylene glycol.[39,46−48] Similar spectral and temporal characteristics were also found for the solvation dynamics of the electron produced by two-photon ionization of other dialcohols.[40,48] Particularly, the wavelength-dependent temporal behavior observed here after electron excitation is in good quantitative agreement with the one after photoexcitation.[39,47] In fact, it was reported that the excess electron in EG is fully solvated at around 50 ps. The slightly longer time of the spectral shift observed here with picosecond pulse radiolysis results mostly from the convolution of the electron pulse duration of about 10 ps and the solvation time.

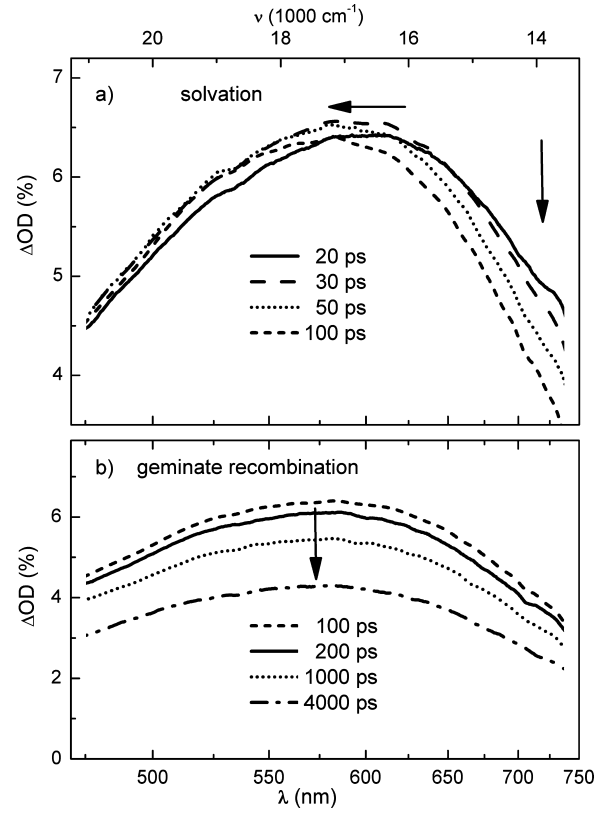

Figure 1. Spectral evolution of the transient absorption in ethylene glycol after picosecond electron radiolysis: spectra at various delay times (a) within the first 100 ps and (b) on the subsequent time scales up to 4 ns.

After formation of the solvated electron, no further spectral changes are observed (see Figure 1b). The observed decay of absorption monitors the depopulation of the solvated electron by geminate recombination with the parent radical cation. The following form of $S(t)$ reproduces the experimental data well in the time window of observation

TABLE 1: Free Energy Change ΔG for the Reduction Reaction of the Metal Cations in H_2O, Reorganization Energy λ_s in H_2O Calculated at Contact Distance d with the Ionic Radius of the Noncomplexed Ion r_{ion}, and the Radius of the Solvated Electron $r_e \approx 2$ Å[a]

parameters	constraints	Cu^{II}	Pb^{II}	Ni^{II}
$-\Delta G$/eV in water		3.02	1.37−1.77	0.17
λ_s/eV		4.5	2.8	4.8
r_{ion}/Å		0.73	1.19	0.69
viscosity/cP (0.2 M)		21.2	20.8	20.8
d/Å	fixed	4	4	4
$\log_{10}$ (A/s^{-1})	8−13	9.82 ± 0.08	9.35 ± 0.07	not defined
b/Å^{-1}	0−3	0.46 ± 0.02	0.57 ± 0.07	not defined
D/10^{-5} cm^2 s^{-1}	0.03−0.34	0.081 ± 0.015	0.090 ± 0.007	not defined
Z	fixed	2	2	2

[a] Dynamic viscosity η in EG derived from measurements on 0.2 M solutions. Parameters obtained by global analysis of the picosecond radiolysis data for the rate constant $k(r) = A \exp[-b(r - d)]$ with charge $Z = 2$.

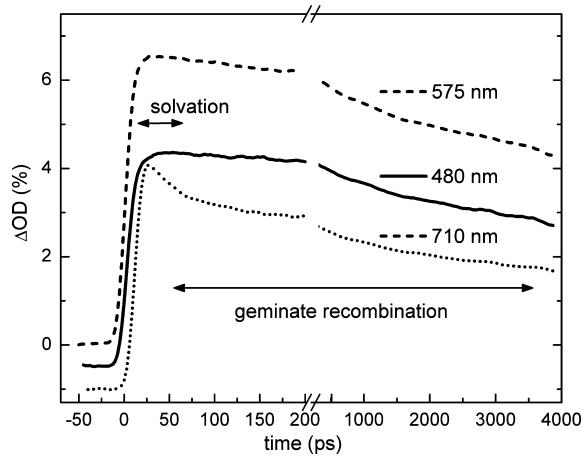

Figure 2. Transient absorption in ethylene glycol after picosecond electron radiolysis traced at the indicated wavelengths. For better visibility, two curves are shifted by 5 ps and 5% ΔOD, respectively. Note the break of the time scale at 200 ps.

$$S(t) = 0.08\exp(-t/0.43) + 0.41\exp(-t/4.87) + 0.5\exp(-t/1000) \quad (12)$$

where t is in nanoseconds. Here the constant of the long time decay was set to 1 μs, the time scale of the overall decay as observed experimentally by nanosecond electron radiolysis (ref 46 and the next section). The precise value of the long time behavior does not have a significant influence on the quality of the fit to the experimental data up to 4 ns. On the time scale of the reduction reaction at high scavenger concentration exhibiting the transient effect within the first hundred of picoseconds (see section IV.3), $S(t)$ is governed by the spur reaction revealed by the ultrafast radiolysis.

IV.2. Decay of the Solvated Electron at Low Concentrations of Metal Cations. The kinetics of the reaction of the solvated electron with homogeneously dispersed metal cations Cu^{2+}, Ni^{2+}, and Pb^{2+} were studied by probing the visible electronic absorption of the solvated electron. We investigated the decay of the absorbance of solvated electrons in neat ethylene glycol and solutions containing metal cations of moderate concentrations in the millimolar range with the nanosecond radiolysis setup. The e_s^- decay in neat ethylene glycol is composed of a first fast part of about 100 ns, due to intraspurs reactions, followed by a slower homogeneous kinetics. The overall decay in ethylene glycol is completed within 2 μs and significantly accelerated by increasing the metal cation concentration. Figure 3 shows the decays of the solvated electron population traced at 575 nm for various concentrations of copper cations. The corresponding kinetics exhibit monoexponential behavior, indicating that the decay follows a pseudo-first-order law. The inset of Figure 3 presents the dependence of the pseudo-first-order rate constants k_{obs} on the concentration of the three metal cations which is linear in the range $0-2 \times 10^{-3}$ mol dm^{-3}. From the slope, the second-order rate constant for the reaction between e^-_{solv} and the metal cation is found to be around $k_2 = (3.0 \pm 0.2) \times 10^9$ dm^3 mol^{-1} s^{-1} for Cu^{2+} and Pb^{2+}. In the case of Ni^{2+} solution the rate constant is slightly lower, $(2.7 \pm 0.2) \times 10^9$ dm^3 mol^{-1} s^{-1}. The same tendency is found in water but with rate constants an order of magnitude higher according to the higher diffusion in water. Moreover, the difference of rate constants of Ni^{2+} relative to the two other systems is in water further enhanced to about 30%. These results point out that the reactions are diffusion controlled for Cu^{2+} and Pb^{2+} whereas thermal activation could start to compete with

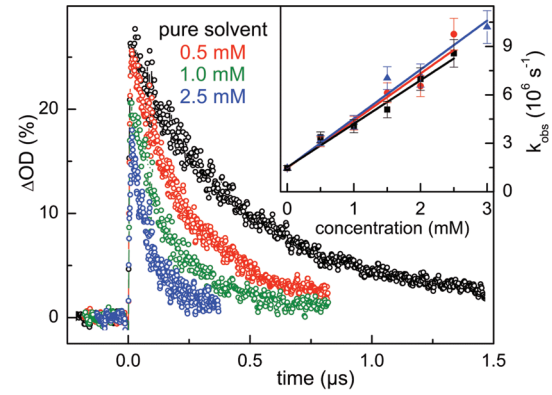

Figure 3. Microsecond decay kinetics of the solvated electron population after nanosecond electron radiolysis traced at its absorption maximum around 575 nm in pure ethylene glycol (black) and in solutions of Cu^{2+} of the indicated concentrations (colors). The inset shows the pseudo-first-order rate constants of the reactions of the solvated electron with Cu^{2+} (red circles), Pb^{2+} (blue triangles), and Ni^{2+} (black squares) at the indicated concentrations in the millimolar range. The straight lines are the best fits with the slopes corresponding to the second-order rate constants of the reactions.

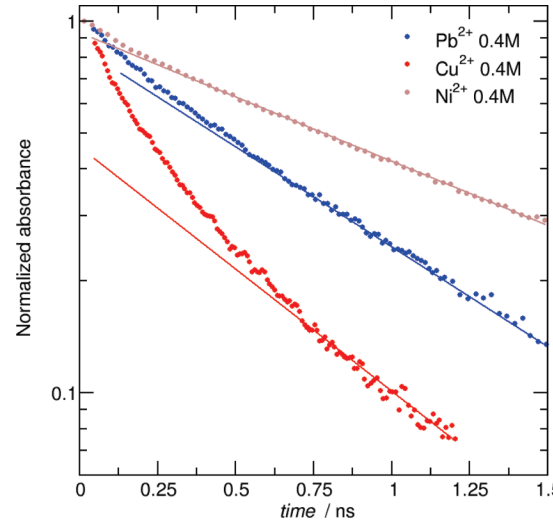

Figure 4. Logarithmically displayed decay kinetics of the solvated electron population traced at its absorption maximum around 575 nm for 0.4 M solutions of Cu^{2+}, Pb^{2+}, and Ni^{2+}. The deviations from the first-order kinetics (straight lines) are due to the transient effect.

diffusion for Ni^{2+}. Therefore, to discriminate the reaction rates for the three metal cations, we need additional information about the rate of the electron transfer reaction.

IV.3. Ultrafast Decay of the Solvated Electron at High Concentrations of Metal Cations. The reduction of the 2-fold charged metal cations by the solvated electron was studied at high concentrations of 0.2 and 0.4 M with the picosecond broadband pulse−probe setup. As in the preceding section the experimental observable to monitor the electron transfer is the absorption of the solvated electron. The transient absorption signal just after electron pulse excitation reveals for all the solutions the same blue shifting and narrowing of the absorption band characteristic to the solvation process. Again, the solvated electron is formed within about 50 ps after the radiolytic excitation.

The kinetics of the solvated electron decay at scavenger concentrations of 0.4 M are shown in Figure 4 for the 3 metal cations in EG. In contrast to the kinetics for low concentration solutions, they are very different for the 3 metal cations. Again, to obtain the best possible signal-to-noise ratio the decay curves

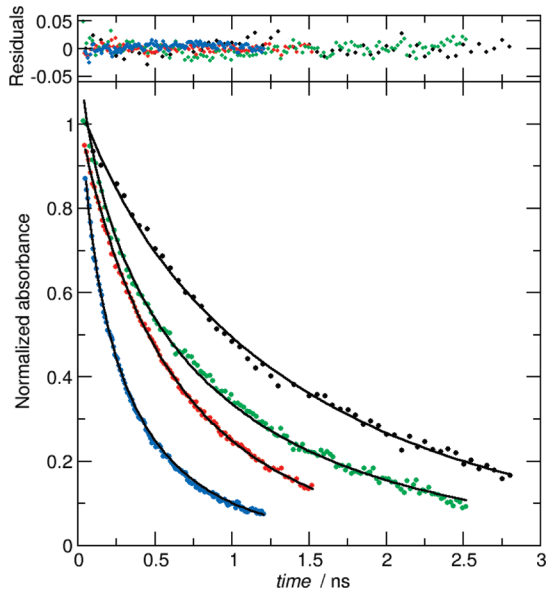

Figure 5. Decay kinetics of the solvated electron population for 0.2 and 0.4 M solutions of Cu^{2+} (blue and green) and Pb^{2+} (red and black). The solid lines are the best fits with parameters *A*, *b*, *D*, and *Z* reported in Table 1.

were traced at the absorption maximum. Here the absorption change is displayed logarithmically, so exponential contributions appear as a straight line. At short time a clear deviation is observed from the exponential behavior. The fastest overall decay is observed for Cu^{2+}, followed by Pb^{2+}, and then Ni^{2+}. The duration of the nonexponential contribution follows the same order: for Cu^{2+}, the transient effect is responsible for 85% of the decay and lasts for 700 ps; these values decrease for Pb^{2+} to 50% and 500 ps, whereas for Ni^{2+} the transient effect is observable for less than 200 ps diminishing the population just by less than 20%. Note that the duration of the transient effect decreases with the concentration of the scavengers (see Figure 5). For nickel there is no observable transient effect at 0.2 M.

It is important to note that the precursors of the solvated electron are scavenged in the presence of a very high concentration of electron acceptor. In fact, the initial transient absorption signal is less intense in the presence of scavengers pointing out that a scavenging reaction takes places during the excitation pulse, i.e., on a time scale of <10 ps. Therefore, the rate of scavenging should be higher than 10^{11} M^{-1} s^{-1}. Such a high rate value is already reported for the precursors of solvated electrons.[49] After the excitation pulse and the consecutive solvation terminated with ~50 ps we observe only the solvated electron and the decay is not affected by the reaction of its electron precursors.

The strongly different kinetics for the three metal ions at same concentration indicates that the overall reaction rate is influenced not only by diffusion but also by electron transfer. The activation barrier to the transfer of solvated electrons to Ni^{2+} is thought to be the rate-limiting factor for this reaction. In contrast, electron transfer to Cu^{2+} is very fast. The plausible reason is the corresponding driving force $-\Delta G$ of the reaction, which is high for reaction with Cu^{2+} and substantially lower for that with Ni^{2+} (Table 1). As the average distance of a solvated electron to its next neighbor metal cation is 8 Å for a concentration of 0.4 M and the penetration depth of the solvated electron in EG is about 4 Å per nanosecond,[50] only a few reactants are in direct initial contact or come into contact during the first nanosecond. As these estimations show, an important part of the reaction that is completed nearly within 1 ns must proceed over a distance over several Angstroms. The same is true for the reaction with Pb^{2+}. The observation of the transient effect points out the occurrence of these long-distance electron transfers. In section IV.4, this will be quantitatively analyzed by taking into account the diffusion of the reactants and the distance dependence of the reaction rate $k(r)$ (see eq 2).

Both the rate and the efficiency of the observed reactions as well as the duration and amplitude of the transient effect are ordered according to the known redox potentials in water ($E°(Cu^{2+}/Cu^{+}) = 0.153$ V, $E°(Pb^{2+}/Pb^{+})$ is estimated between −1.5 and −1.1 V and $E°(Ni^{2+}/Ni^{+})$ is estimated to be −2.7 V).[51,52] The corresponding free enthalpy changes of the reaction calculated with the known redox potential of the solvated electron ($E°(H_2O/e_s^-) = -2.87$ V) and ionic radius[53] are listed in Table 1. This indicates a dependence of the reaction rate and the reaction radius on the free enthalpy change of the reaction as revealed for other donor/acceptor systems.[19,20,28] The application of $k(r)$ based on the Marcus expression will be discussed in the last part of this work.

IV.4. Data Analysis and Discussion. The formation of e_s^- almost ends 50 ps after excitation in ethylene glycol. Thus, analysis of the transient effect was done for the data in a temporal range from ~50 ps after the excitation pulse according to the procedure described in section III. For that purpose, four parameters have to be adjusted, *A*, *b*, *D*, and *Z*, the unknown effective charge of the scavenger in the concentrated solutions. In a first stage of data analysis, we fixed the charge of the scavenger to $Z = 2$, meaning that the metal cations are not complexed by the counterions ClO_4^-; at the end we will discuss the charge effect.

Diffusion Coefficient. It is not so obvious to find the value of the diffusion coefficient of the solvated electrons in ethylene glycol. This value can be determined by conductivity measurements or by scavenging experiments assuming that the observed reaction of the solvated electron can be considered as completely diffusion controlled. In the first method the mobility of the solvated electron is measured and the diffusion coefficient is deduced using the Nernst−Einstein equation. Conductivity measurements contain usually large errors, and the scavenging method gives always a too large value of *D*. The reason is that even at low scavenger concentration the reaction can occur at larger distance than contact distance. The only experimental value reported for the solvated electron mobility in ethylene glycol is 2.8×10^{-5} cm^2 V^{-1} s^{-1}. This value gives $D = 0.72 \times 10^{-5}$ cm^2 s^{-1}.[54] The diffusion coefficient of the hydrated electron is around 4.8×10^{-5} cm^2 s^{-1}. If we simply take into account the high viscosity of ethylene glycol which is 20 times higher than that of water, we should find $D = 0.27 \times 10^{-5}$ cm^2 s^{-1} in EG, which is three times lower than the value of 0.72×10^{-5} cm^2 s^{-1} found by conductivity measurements. It was reported that for a polar solvent the diffusion constant of the solvated electron is related to the self-diffusion coefficient of the solvent molecules. In the case of ethylene glycol, the diffusion coefficient of the solvated electron was derived by the correlation relationship to be 0.09×10^{-5} cm^2 s^{-1}.[55] This value is much lower than the previously reported value of 0.72×10^{-5} cm^2 s^{-1}. Pulse radiolysis measurements showed that the rate constant of the reaction between the solvated electrons and silver ions in ethylene glycol is 3×10^9 mol L^{-1} s^{-1}.[56] As reported for water, this reaction is controlled by diffusion. By assuming a reaction radius of 3 Å, we find that the mutual diffusion coefficient in ethylene glycol is 0.19×10^{-5} cm^2 s^{-1}. As the diffusion constant of the metal ions is lower than that of e_{solv}^-,

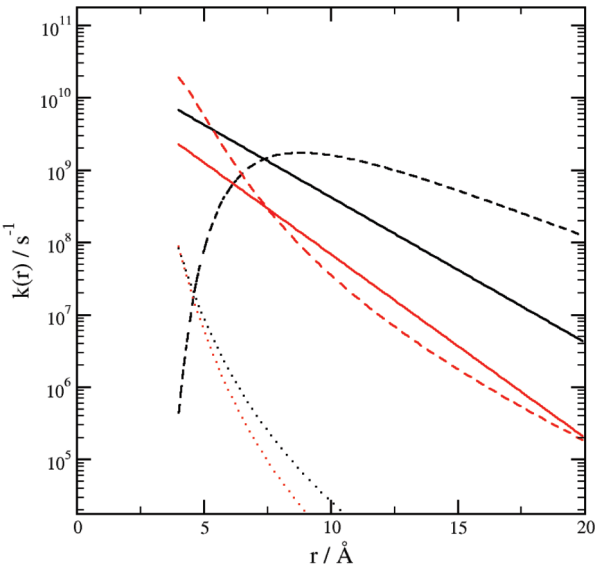

Figure 6. Distance dependence of the rate $k(r)$ for reaction of the solvated electron with Pb^{2+}(red) and Cu^{2+} (black). The solid lines are calculated according to $k = A \exp[-b(r - d)]$ with the values reported in Table 1, dotted and dashed lines according to the Marcus equation with the ionic radii reported in Table 1 and with those set to 2 Å, respectively.

we consider that the value of the diffusion coefficient of the solvated electron in EG is lower than 0.19×10^{-5} cm^2 s^{-1} and then it is again much lower than the reported one (0.72×10^{-5} cm^2 s^{-1}). Moreover, we can estimate the D value for the solvated electron according to the Stokes−Einstein equation given by

$$D = \frac{kT}{x\pi r\eta} \tag{13}$$

where x is equal 6 when the size of the solvent is small and x is around 2.5 in the case of EG, η is the viscosity of the solvent, and r is the radius of the solute.[57] At 22.5 °C, the measured value of the viscosity of the solvent containing 0.2 and 0.4 M metal cations is 21 and 24 cP, respectively. According to these experimental values and by considering a radius of the solvated electron equal to 2 Å, the D of e_s^- should be around 0.13 and 0.11×10^{-5} cm^2 s^{-1}. As we can see, the value for D of e_{solv}^- in EG is not well determined from the different data given in the literature. Therefore, in the present work D is considered as an adjustable parameter ranging between 0.03×10^{-5} and 0.34×10^{-5} cm^2 s^{-1}. This corresponds to a 99% confidence interval of the log-normal distribution LogN(0.1,1.5) as used for prior pdf for D (see section III.2).

Distance-Dependent Rate Constant. The decays calculated using eqs 1−3 were fitted to the experimental decays using eqs 7, 9, and 10, and the best fits and residuals are shown in Figure 5 for two concentrations of copper and lead. In the case of the nickel systems, the fits are unsuccessful and the parameters cannot be deduced with the simulations. This fact is understandable as the transient effect is very small even at 0.4 M Ni^{2+}, and the reaction seems to occur only at contact distance. For copper and lead, the residuals are low and no correlation is apparent, showing that the model reproduces correctly the experimental observation. The parameters A, b, and D are deduced and reported in Table 1. We note that the values of D for the copper and lead system are very close and in good agreement with those reported in the literature and discussed above. The value of b is 0.46 and 0.57 Å^{-1} for copper and lead,

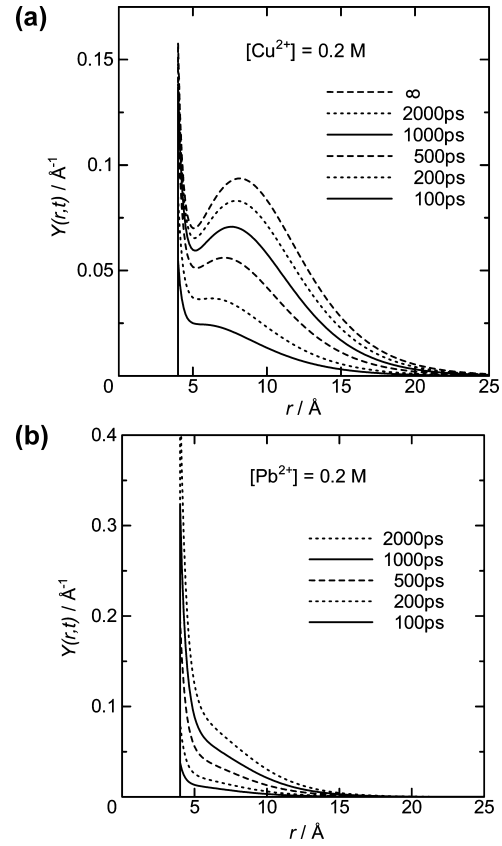

Figure 7. Distribution of the reaction distance for a scavenger concentration of 0.2 M of (a) Cu^{2+} and (b) Pb^{2+} at the indicated times.

respectively. With the deduced A and b, the distance-dependent reaction rate $k(r)$ (eq 3) is depicted in Figure 6. The first-order distance-dependent rate constant, compared to the reaction time (around 1 ns) is not negligible even at a long distance around 1 nm. The value of $k(r)$ is higher for copper than for lead. The high values of $k(r)$ show that the electron transfer reaction occurs also at distance as long as 10 Å, but it is negligible at a distance over around 15 Å.

Distribution of Reaction Distance. The distribution of reaction distance $Y(r)$ is calculated from eq 5 and displayed in Figure 7a and 7b for different reaction times for the systems containing 0.2 M Cu^{2+} and 0.2 M Pb^{2+}. At short time the reaction occurs at short distance, and then the distribution shifts gradually to longer distances as expected. Just after generation of the solvated electrons, the distribution of solvated electrons and scavenger ions is random and the distances between them are also random. A short time after generation, solvated electron-scavenger ion pairs with short distance react first because $k(r)$ is larger at short distances. As time proceeds, the number of such pairs decreases and the reaction shifts to pairs with longer distances.

Although A and b are independent of the scavenger concentration, the distribution of reaction distance $Y(r)$ (eq 4) depends on the initial concentration of metal cation. Figure 8 reports $Y(r)$ for copper at two concentrations. As the concentration increase from 0.2 to 0.4 M, the maximum of the reaction distance shifts to smaller values. This occurs because at higher concentrations there are more pairs with shorter distances than at lower concentrations. For a given concentration, the reaction occurs at a longer distance for copper than for lead.

Charge Effect. It is reported that the metal cations at high concentration could be complexed by counteranions. The

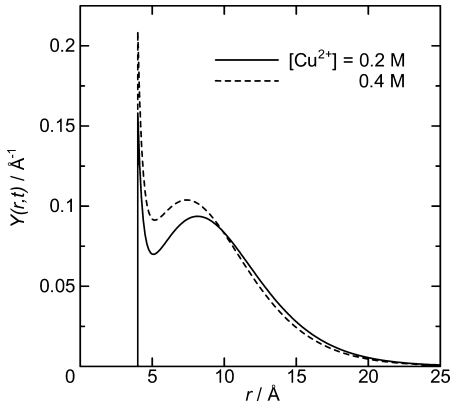

Figure 8. Distribution of the reaction distance for 0.2 and 0.4 Cu^{2+}.

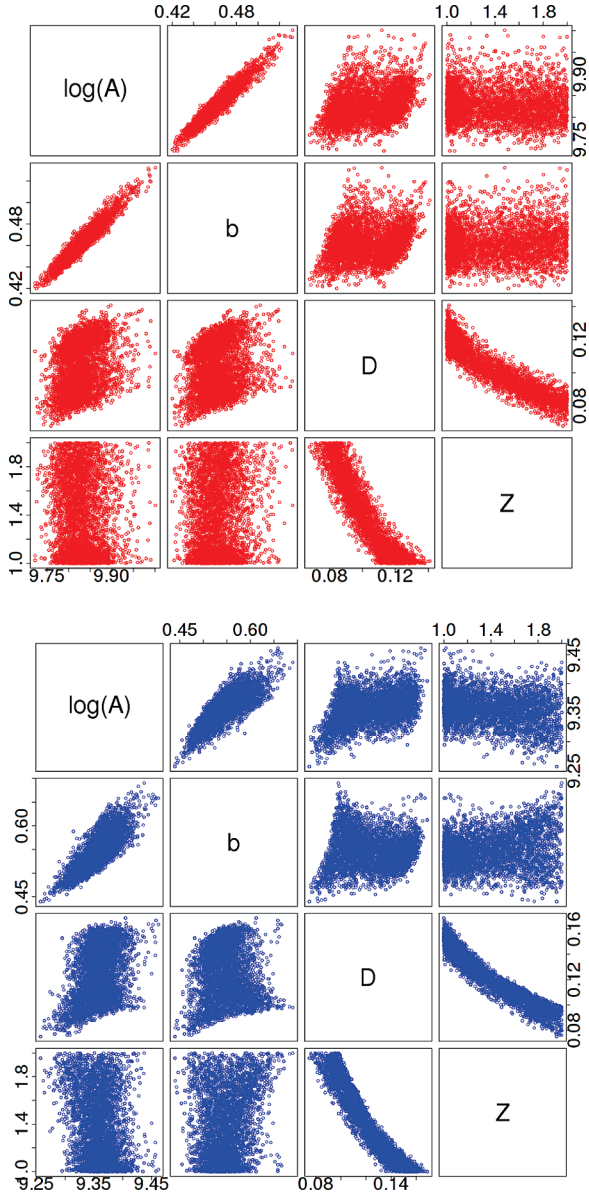

Figure 9. Sample of posterior pdf of A, b, D, and Z for the reaction of the solvated electron with Pb^{2+} (blue) and Cu^{2+} (red).

perchlorate anion is one of the most inert counterions in water, but in alcohol a complexation between ClO_4^- and Cu^{2+} and Pb^{2+} can occur due the lower dielectric constant.[58] In that case, the effective charge seen by the solvated electron can be lower

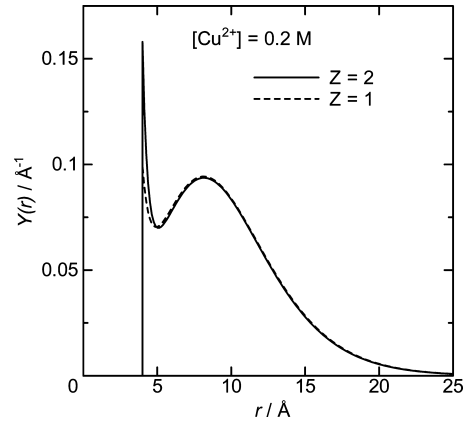

Figure 10. Distribution of the reaction distance for 0.2 M of Cu^{2+} derived for a charge $Z = 1$ and 2, respectively.

than 2. For that reason, we performed data analysis with a charge variable between one and two. Figure 9 reports the corresponding parameter spaces obtained by Bayesian data analysis. There is a strong correlation between Z and D, and all values of Z between 1 and 2 provide good fit of the data. For copper, D varies from 0.08×10^{-5} to 0.12×10^{-5} cm^2 s^{-1} when Z varies from 2 to 1 (Tables 1 and 2, Figure 9a). These values of D are still within the range reported in the literature and discussed above. Therefore, it is not possible to conclude about the value of Z. The average value of Z is 1.3 (Table 3). For a given solvated electron decay, a decrease in scavenger charge is compensated by an increase of the diffusion coefficient as diffusion and electrostatic interaction are coupled physically. At first order, eq 2 shows that the charge Z is only involved through its product with D. By contrast, the other parameters A and b are very weakly correlated to Z.

Figure 10 shows that Z has a very minor effect on the distribution $Y(r)$ of reaction distance. In fact, as $k(r)$ is almost independent of Z and the low value of Z is compensated by a high value of D, the distance distribution remains almost unchanged except for distances very close to contact. The reduction of the peak toward the contact radius is due to the reduced attractive electrostatic potential for $Z = 1$.

Comparison to Marcus Theory. Finally, it is interesting to compare the distance-dependent rate constant k deduced from the fits with that given by Marcus theory. The theory of electron transfer reactions was described first by R. A. Marcus[59,60] and allows expressing the rate constant of the solvated electron in terms of the standard reduction potentials of the reactants. The Marcus equation (eq 14) is very often used to discuss the rate of electron transfer reactions. It gives the first-order electron transfer rate $k(r)$

$$k(r) = \frac{2\pi}{\hbar} J_0^2 \exp[-\beta(r - r_0)] \frac{1}{\sqrt{4\pi\lambda k_B T}} \exp\left[-\frac{(\Delta G + \lambda)^2}{4\lambda k_B T}\right] \quad (14)$$

where J_0 is the electronic coupling matrix element at $r = r_0$, β its attenuation coefficient, ΔG the free enthalpy change of the reaction, and λ_s the solvent reorganization energy

$$\lambda_s = \frac{e^2}{2}\left(\frac{1}{\varepsilon_{op}} - \frac{1}{\varepsilon_s}\right)\left(\frac{1}{r_e} + \frac{1}{r_s} - \frac{2}{r}\right) \quad (15)$$

TABLE 2: Parameters Obtained for the Rate Constant $k(r) = A \exp[-b(r - d)]$ with $Z = 1$

parameters	constraints	Cu^{II}	PbII	Ni^{II}
d/Å	fixed	4	4	4
$\log_{10}$ (A/s^{-1})	8−13	9.83 ± 0.04	9.36 ± 0.04	Not defined
b/Å^{-1}	0−3	0.46 ± 0.02	0.52 ± 0.05	Not defined
D/10^{-5} cm^2 s^{-1}	0.03−0.34	0.12 ± 0.01	0.15 ± 0.01	Not defined
Z	fixed	1	1	1

TABLE 3: Parameters Obtained for the Rate Constant $k(r) = A \exp[-b(r - d)]$ with Variable Z

		prior pdf	estimation	correlation matrix		
Cu^{II}	A	Logunif(10^8,10^{13})	9.830 ± 0.037			
	b	Unif(0,3)	0.462 ± 0.015	0.96		
	D	Lognorm(0.1,1.5)	0.107 ± 0.016	0.28	0.19	
	Z	Unif(1,2)	1.31 ± 0.32	−0.05	0.95	−0.93
Pb^{II}	A	Logunif(10^8,10^{13})	9.359 ± 0.027			
	b	Unif(0,3)	0.548 ± 0.037	0.79		
	D	Lognorm(0.1,1.5)	0.128 ± 0.023	0.40	0.01	
	Z	Unif(1,2)	1.34 ± 0.32	−0.26	0.21	−0.96

where ε_{op} and ε_s are the optical and static dielectric constants of the solvent and r_e and r_s the radii of solvated electron and the scavenger, respectively.

The distance dependence of the Marcus equation is also plotted in Figure 6 for reactions of the solvated electron with electron scavengers Cu^{2+} and Pb^{2+} ions. The parameter values assumed are $J_0 = 10$ cm^{-1} at 4 Å, $\beta = 0.3$ Å^{-1}, and $r_e = 2.0$ Å. Since λ_s depends on r_e and r_s and r_s can change with Z, two values of r_s were assumed for each scavenger ion: those of bare ions, 0.73 and 1.19 Å for Cu^{2+} and Pb^{2+}, respectively, and 2 Å. β was set to be 0.3 Å^{-1} because at longer distances it gives plots with slopes similar to those obtained from experiment. However, as seen in Figure 6, the theoretical curves are far from the experimental curves. The effect of the radius of solvated electron scavengers is very strong on the rate of electron transfer. In fact, the reorganization energy depends on that radius. Therefore, the rate constant given by Marcus theory depends drastically on the thermodynamics of electron transfer. As the distance-dependent rate constant given by the Marcus equation obtained with small radii for ions are very far from the experimental values (Figure 6), we can consider that in our solutions the ions are not bare. For conclusions based on the Marcus equation we need to know more precisely the value of the enthalpy change and of the solvent reorganization energy of electron transfer. For that purpose it is important to get knowledge on the structure of the ions in solutions.

Conclusion

For the first time the transient effect for solvated electron scavenging at room temperature is measured by picosecond pulse radiolysis with the electron-pulse−pump/white-light-continuum-probe setup. Data analysis reveals that long-range electron transfer is possible and that a barrierless reaction of the solvated electron does not necessarily occur at contact distance. Among the three solvated electron scavengers displaying different free enthalpy change in the reduction reaction, the copper system, which constitutes a very exothermic reaction, presents the strongest transient effect. In that case, the reaction between the solvated electron and copper can occur at long distance on the order of 10 Å. In contrast, the reaction with nickel that exhibits the lowest free enthalpy change does not reveal almost any transient effect even for 0.4 M scavenger concentration. The electron transfer to nickel is not fully controlled by diffusion and occurs only at contact distance. It is interesting to focus on the Marcus equation to express the distance-dependent rate constant by more detailing the reorganization energy and free enthalpy change of the reactions. Molecular simulations could be helpful to further elucidate the possible complexation with the counteranions of the metal scavengers and so to obtain the parameters involved in the Marcus equation.

References and Notes

(1) Hart, E. J.; Boag, J. W. *J. Am. Chem. Soc.* **1962**, *84*, 4090.
(2) Keene, J. W. *Nature* **1963**, *197*, 47.
(3) Dorfman, L. M.; Jou, F. Y. Optical absorption spectrum of the solvated electron in ethers and in binary liquid systems. In *Electrons in Fluids*; Jortner, J., Kestner, N. R., Eds.; Springer: New York, 1972; pp 447−457.
(4) Jou, F. Y.; Dorfman, L. M. *J. Chem. Phys.* **1973**, *58*, 4715.
(5) Ferradini, C.; Jay-Gerin, J. P. *Radiat. Phys. Chem.* **1996**, *48*, 473.
(6) Belloni, J.; Marignier, J. L. *Radiat. Phys. Chem.* **1989**, *34*, 157.
(7) Mostafavi, M.; Lampre, I. An Overview of Solvated Electrons: Recent Advances. In *Recent Trends in Radiation Chemistry*; Wishart, J. F., Rao, B. S. M., Eds.; World Scientific Publishing Co.: Singapore, 2009; pp 21−58.
(8) Larsen, R. E.; Glover, W. J.; Schwartz, B. J. *Science* **2010**, *329*, 65.
(9) Siefermann, K. R.; Liu, Y.; Lugovoy, E.; Link, O.; Faubel, M.; Buck, U.; Winter, B.; Abel, B. *Nat. Chem.* **2010**, *2*, 274.
(10) Buxton, G. V.; Greenstock, C. L.; Helman, W. P.; Ross, A. B. *J. Phys. Chem. Ref. Data* **1988**, *17*, 513.
(11) Das, R.; Periasamy, N. *Chem. Phys.* **1989**, *136*, 361.
(12) Angel, S. A.; Peters, K. S. *J. Phys. Chem.* **1989**, *93*, 713.
(13) Angel, S. A.; Peters, K. S. *J. Phys. Chem.* **1991**, *95*, 3603.
(14) Nishikawa, S.; Asahi, T.; Okada, T.; Mataga, N.; Kakitani, T. *Chem. Phys. Lett.* **1991**, *185*, 237.
(15) Song, L.; Dorfman, R. C.; Swallen, S. F.; Fayer, M. D. *J. Phys. Chem.* **1991**, *95*, 3454.
(16) Song, L.; Swallen, S. F.; Dorfman, R. C.; Weidemaier, K.; Fayer, M. D. *J. Phys. Chem.* **1993**, *97*, 1374.
(17) Scully, A. D.; Hirayama, S.; Hachisu, D.; Tominaga, T. *J. Phys. Chem.* **1992**, *96*, 7333.
(18) Scully, A. D.; Hirayama, S.; Fukushima, K.; Tominaga, T. *J. Phys. Chem.* **1993**, *97*, 10524.
(19) Stevens, B.; Biver III, C. J. *Chem. Phys. Lett.* **1994**, *226*, 268.
(20) Murata, S.; Nishimura, M.; Matsuzaki, S. Y.; Tachiya, M. *Chem. Phys. Lett.* **1994**, *219*, 200.
(21) Iwai, S.; Murata, S.; Tachiya, M. *J. Chem. Phys.* **1998**, *109*, 5963.
(22) Murata, S.; El-Kemary, M.; Tachiya, M. *Int. J. Photoenergy* **2008**, 150682.
(23) Allonas, X.; Jacques, P.; Accary, A.; Kessler, M.; Heisel, F. *J. Fluoresc.* **2000**, *10*, 237.
(24) Kikuchi, K.; Katagiri, T.; Niwa, T.; Takahashi, Y.; Suzuki, H.; Ikeda, H.; Miyashi, T. *Chem. Phys. Lett.* **1992**, *193*, 155.
(25) Murata, S.; Matsuzaki, S. Y.; Tachiya, M. *J. Phys. Chem.* **1995**, *99*, 5354.
(26) Murata, S.; Tachiya, M. *J. Chim. Phys.* **1996**, *93*, 1577.
(27) Murata, S.; Tachiya, M. *J. Phys. Chem.* **1996**, *100*, 4064.
(28) Burel, L.; Mostafavi, M.; Murata, S.; Tachiya, M. *J. Phys. Chem. A* **1999**, *103*, 5882.

(29) Belloni, J.; Monard, H.; Gobert, F.; Larbre, J.-P.; Demarque, A.; De Waele, V.; Lampre, I.; Marignier, J.-L.; Mostafavi, M.; Bourdon, J. C.; Bernard, M.; Borie, H.; Garvery, T.; Jacquemard, B.; Leblond, B.; Lepercq, P.; Omeich, M.; Roch, M.; Rodier, J.; Roux, R. *Nucl. Instrum. Methods, A* **2005**, *539*, 527.

(30) Marignier, J. L.; De Waele, V.; Monard, H.; Gobert, F.; Larbre, J.-P.; Demarque, A.; Mostafavi, M.; Belloni, J. *Radiat. Phys. Chem.* **2006**, *75*, 1024.

(31) Schmidhammer, U.; De Waele, V.; Marquès, J.-R.; Bourgeois, N.; Mostafavi, M. *Appl. Phys. B: Laser Opt.* **2009**, *94*, 95.

(32) De Waele, V.; Schmidhammer, U.; Marquès, J.-R.; Monard, H.; Larbre, J.-P.; Bourgeois, N.; Mostafavi, M. *Radiat. Phys. Chem.* **2009**, *78*, 1099.

(33) Belloni, J.; Crowell, R. A.; Katsumura, Y.; Lin, M.; Marignier, J. L.; Mostafavi, M.; Muroya, Y.; Akinori, S.; Tagawa, S.; Yoshida, Y. De Waele, V.; Wishart, J. F. In Recent Trends in Radiation Chemistry, Eds. Wishart, J. F. And Rao, B. S. World Scientific: River Edge, NJ, 2010; p121.

(34) De Waele, V.; Sorgue, S.; Pernot, P.; Marignier, J. L.; Monard, H.; Larbre, J. P.; Mostafavi, M. *Chem. Phys. Lett.* **2006**, *423*, 30.

(35) Atinault, E.; De Waele, V.; Schmidhammer, U.; Fattahi, M.; Mostafavi, M. *Chem. Phys. Lett.* **2008**, *460*, 461.

(36) Belloni, J.; Billian, F.; Cordier, C.; Delaire, J. A.; Delcourt, M. O. *J. Phys. Chem.* **1978**, *82*, 532.

(37) Tachiya, M. *Radiat. Phys. Chem.* **1983**, *21*, 167.

(38) Sano, H.; Tachiya, M. *J. Chem. Phys.* **1979**, *71*, 1276.

(39) Soroushian, B.; Lampre, I.; Bonin, J.; Pernot, P.; Pommeret, S.; Mostafavi, M. *J. Phys. Chem. A* **2006**, *110*, 1705.

(40) Bonin, J.; Lampre, I.; Pernot, P.; Mostafavi, M. *J. Phys. Chem. A* **2007**, *111*, 4902.

(41) Gregory, P. C. *Bayesian logical data analysis for the physical sciences*; Cambridge University Press: Cambridge, U.K., 2005.

(42) Gelman, A.; Carlin, J.; Stern, H.; Rubin, D. *Bayesian Data Analysis*, 2nd ed.; Chapman & Hall: New York, 2004.

(43) Ruthmann, J.; Kovalenko, S. A.; Ernsting, N. P.; Ouw, D. *J. Chem. Phys.* **1998**, *109*, 5466.

(44) Schmidhammer, U.; Megerle, U.; Lochbrunner, L.; Riedle, E.; Karpiuk, J. *J. Phys. Chem. A* **2008**, *112*, 8487.

(45) Horng, M. L.; Gardecki, J. A.; Papazyan, A.; Maroncelli, M. *J. Phys. Chem.* **1995**, *99*, 17311.

(46) Lin, M.; Mostafavi, M.; Muroya, Y.; Han, Z.; Lampre, I.; Katsumura, Y. *J. Phys. Chem. A* **2006**, *110*, 11404.

(47) Soroushian, B.; Lampre, I.; Pernot, P.; De Waele, V.; Pommeret, S.; Mostafavi, M. *Chem. Phys. Lett.* **2004**, *394*, 313.

(48) Lampre, I.; Bonin, J.; Soroushian, B.; Pernot, P.; Mostafavi, M. *J. Mol. Liq.* **2008**, *141*, 124.

(49) Pommeret, S.; Gobert, F.; Mostafavi, M.; Lampre, I.; Mialocq, J.-C. *J. Phys. Chem. A* **2001**, *105*, 11400.

(50) The penetration depth $r = (2Dt)^{0.5}$ per time t is calculated with the diffusion coefficient D estimated to be 0.1×10^{-5} cm^2 s^{-1} (see section IV.3).

(51) Lide, D. R. *Handbook of Chemistry and Physics*, 75th ed.; CRC Press: Boca Raton, FL, 1994.

(52) Baxendale, J. H.; Dixon, R. S. *Z. Phys. Chem.* **1964**, *43*, 161.

(53) Shannon, R. D. *Acta Crystallogr. Sect. A* **1976**, *32*, 751.

(54) Jay-Gerin, J. P.; Ferradini, C. J. *Chim. Phys.* **1994**, *91*, 173.

(55) Krebs, P. *Z. Phys. Chem.* **2000**, *214*, 1348.

(56) Soroushian, B.; Lampre, I.; Belloni, J.; Mostafavi, M. *Radiat. Phys. Chem.* **2005**, *72*, 111.

(57) Kooijman, H. A. *Ind. Eng. Chem. Res.* **2002**, *41*, 3326.

(58) Doe, H.; Kitagawa, T. *Bull. Chem. Soc. Jpn.* **1985**, *58*, 2975.

(59) Marcus, R. A. *J. Chem. Phys.* **1956**, *24*, 966.

(60) Marcus, R. A. *Annu. Rev. Phys. Chem.* **1964**, *15*, 155.

JP107278W